

Markov propagation of allosteric effects in biomolecular systems: application to GroEL–GroES

Chakra Chennubhotla and Ivet Bahar*

Department of Computational Biology, School of Medicine, University of Pittsburgh, Pittsburgh, PA, USA

* Corresponding author. Department of Computational Biology, School of Medicine, University of Pittsburgh, Biomedical Science Tower 3, Fifth Avenue, Pittsburgh, PA 15213, USA. Tel: +1 412 648 3332; Fax: +1 412 648 3163; E-mail: bahar@cceb.pitt.edu

Received 6.12.05; accepted 11.5.06

We introduce a novel approach for elucidating the potential pathways of allosteric communication in biomolecular systems. The methodology, based on Markov propagation of ‘information’ across the structure, permits us to partition the network of interactions into soft clusters distinguished by their coherent stochastics. Probabilistic participation of residues in these clusters defines the communication patterns inherent to the network architecture. Application to bacterial chaperonin complex GroEL–GroES, an allostery-driven structure, identifies residues engaged in intra- and inter-subunit communication, including those acting as *hubs* and *messengers*. A number of residues are distinguished by their high potentials to transmit allosteric signals, including Pro33 and Thr90 at the nucleotide-binding site and Glu461 and Arg197 mediating inter- and intra-ring communication, respectively. We propose two most likely pathways of signal transmission, between nucleotide- and GroES-binding sites across the *cis* and *trans* rings, which involve several conserved residues. A striking observation is the opposite direction of information flow within *cis* and *trans* rings, consistent with negative inter-ring cooperativity. Comparison with collective modes deduced from normal mode analysis reveals the propensity of global hinge regions to act as messengers in the transmission of allosteric signals.

Molecular Systems Biology 4 July 2006; doi:10.1038/msb4100075

Subject Categories: structural biology; proteins

Keywords: allosteric effects; chaperonins; information propagation; Markov process; network model

Introduction

A central goal in structural biology is to understand the mechanism of allosteric communication in supramolecular systems. Allostery is the cooperative process by which local effects propagate across the structure, often to regions spatially distant from initiation sites. A prime example of allostery is the transition of hemoglobin from low-affinity (T; tense) to high-affinity (R; relaxed) state upon oxygen binding. Two classical models have been proposed to describe allosteric transitions in such multimeric proteins: the Monod–Wyman–Changeux (MWC) (Monod *et al.*, 1965) and Koshland–Nemethy–Filter (KNF) (Koshland *et al.*, 1966) models. The former assumes a concerted, all-or-none change in all subunits, whereas the latter allows for the sequential transition of individual subunits. Although these models, and more complicated ones, are still being debated, the emerging view from experimental and computational studies is that many regulatory multimeric proteins, and in particular allosteric enzymes, possess the *intrinsic ability* to undergo MWC-like changes in structure, conferred by their three-dimensional (3-d) network of inter-residue interactions (in the absence of ligands). Such cooperative effects, enhanced by structural symmetry in the case of oligomers (Changeux and Edelstein, 2005), are usually triggered or stabilized upon ligand binding at particular

susceptible sites (Tobi and Bahar, 2005). Recent computational studies also lend support to the intrinsic role of inter-residue contact topology in defining functional dynamics (Bahar and Rader, 2005; Ma, 2005). Yet, the pathways of signal transduction favored by the network of inter-residue contacts in supramolecular structures remain to be established.

The allostery-driven system we explore here is the bacterial chaperonin system GroEL–GroES, a widely studied molecular chaperone that assists folding of a subset of *Escherichia coli* proteins (Thirumalai and Lorimer, 2001; Saibil and Ranson, 2002; Horovitz and Willison, 2005). GroEL has a cylindrical structure, 150 Å long and 140 Å wide, consisting of 14 identical chains/subunits organized in two back-to-back stacked rings of seven subunits each (Xu *et al.*, 1997) (Figure 1). Each chain is composed of three domains, equatorial (E1 and E2), intermediate (I1 and I2) and apical (A), sequentially ordered as E1–I1–A–I2–E2. During the allosteric cycle that mediates protein folding, the rings alternate between open (*cis*) and closed (*trans*) forms in an ATP-regulated manner, providing access to, or release from, the central cavity where the folding of encapsulated (partially folded or misfolded) protein/peptide is assisted.

Chaperonin function requires an efficient communication between distant locations on the complex. For example, ATP binding to E-domains is accompanied by a cooperative

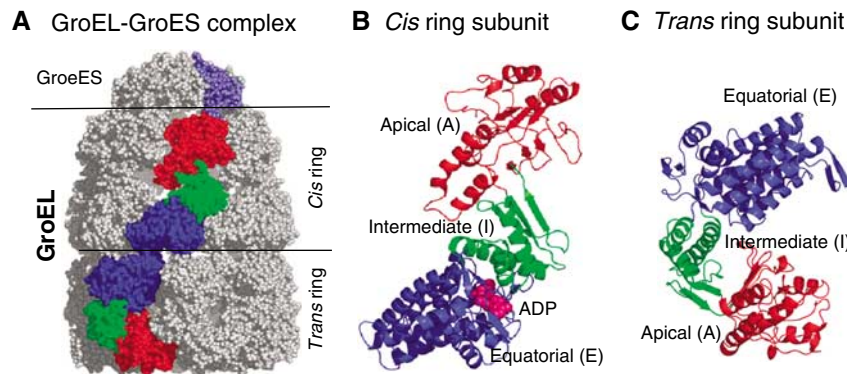


Figure 1 Structure of the GroEL–GroES complex. **(A)** Space-filling model from the crystal structure determined by Xu *et al* (1997) (Protein Data Bank (PDB): 1AON). GroEL has a cylindrical structure, composed of two rings, termed the *cis* and *trans* rings, depending on the position of the GroES cap. Each ring in GroEL is composed of seven subunits. One subunit in each ring is shown in color (red, green and blue) in **(A)**, along with one of the chains of the heptameric co-chaperonin (shown in gray/slate). The colored subunits on the GroES cap and the GroEL *cis* and *trans* rings correspond to three representative chains (identified as chains R, D and K in the PDB file (Berman *et al*, 2000)) whose communication dynamics will be examined below (see Figure 3C). **(B)** and **(C)** display ribbon diagrams of these two subunits belonging to the *cis* and *trans* rings, respectively. Each subunit consists of three domains, A, I and E, which refer to the apical, intermediate and equatorial domains, respectively. The corresponding residue ranges are: [A] Met193–Gly375; [I] Cys138–Gly192 (I1) and Val376–Gly410 (I2); and [E] Met1–Pro137 (E1) and Val411–Pro525 (E2). ADP molecule bound to the equatorial domain of the *cis* ring subunit is displayed in pink in panel B.

conformational change (T→R) that facilitates the binding of co-chaperonin GroES at the A-domains in the same (*cis*) ring, whereas substrate binding and ATP binding to opposite (*trans*) ring triggers the release of GroES, substrate protein and ADP from the *cis* ring. Although several studies have been undertaken to unravel the mechanism of allostery in GroEL–GroES (Xu *et al*, 1997; Ma and Karplus, 1998; Sigler *et al*, 1998; de Groot *et al*, 1999; Ma *et al*, 2000; Thirumalai and Lorimer, 2001; Kass and Horovitz, 2002; Keskin *et al*, 2002; Horovitz and Willison, 2005), the underlying pathways of allosteric communication remain to be elucidated, as well as the key interactions that mediate the intra-ring (positive) and inter-ring (negative) cooperativity.

In this paper, we introduce a novel approach for unraveling potential pathways of signal transduction in large structures. Motivated by the recent success of network-based approaches in exploring structural motifs/mechanisms for allosteric communication (Keskin *et al*, 2002; Xu *et al*, 2003), we model structures as networks of residues (Bahar *et al*, 1997; Haliloglu *et al*, 1997; Hinsen, 1998; Doruker *et al*, 2000; Atilgan *et al*, 2001) and study the Markov propagation of ‘information’ across these networks. We rely on the premise that signaling/communication ability is an intrinsic property of the 3-d structure and that naturally selected structures are those predisposed to optimally meet these functional requirements. We show how a Markovian network formalism based on information theory (Kullback, 1959; McLachlan and Basford, 1988; Chennubhotla and Jepson, 2005) and spectral graph methods (Chung, 1997) helps understand the pathways of communication between spatially distant sites and significantly reduces the complexity of the problem. In particular, we analyze how information diffuses between ATP-binding and GroES-binding sites in GroEL–GroES.

Our approach is structure-based, rather than sequence-based (Lock-less and Ranganathan, 1999; Kass and Horovitz, 2002; Stan *et al*, 2003; Suel *et al*, 2003), in that it maps a full-atom representation into a hierarchy of networks of decreasing

resolution, performs the analysis of dominant patterns in reduced space(s) and reconstructs the detailed models with a minimal loss of information (Figure 2). Such dimensionality reduction algorithms based on Markov propagation stochastics expressed in terms of Fokker–Planck operator have been shown to convey useful information on the diffusion processes in complex systems (Bahar *et al*, 1994; Coifman *et al*, 2005; Nadler *et al*, 2006). The communication properties at different levels of the hierarchy allow for partitioning the complex structure into *soft* clusters. The probabilistic distribution of amino acids in these clusters, or the so-called ownership of residues by the clusters, permits us to evaluate the communication entropies of individual residues. Residues distinguished by high entropies possess a high potential to transmit allosteric signals, hence their identification as sites of large *allosteric potential* (Ming and Wall, 2005).

Notably, our analysis provides evidence for the critical role played by the GroES mobile loops Glu18–Ala33 in establishing the communication with GroEL *cis* ring. Also, we identify the residues that establish positive intra-ring cooperativity. Negative cooperativity between the two rings is suggested by the tendency of the two rings to engage in intra-ring communication of opposite rotational direction. The *cis* ring E-domains exhibit stronger intra-ring coupling than their *trans* ring counterparts in the presently examined ADP-bound complex, and they unambiguously emerge as centers with the highest propensity for ‘broadcasting’ perturbations to the entire structure. Finally, we identify residues acting as *hubs* and/or *messengers* for collecting and passing information across the network and we determine *maximum likelihood communication pathways* from nucleotide-binding site to co-chaperonin mobile loop across the rings. A significant property that emerges from the comparison of the present results with those from normal mode analysis of GroEL–GroES collective dynamics is the propensity of the global hinge sites identified with the Gaussian network model (GNM) (Bahar *et al*, 1997; Haliloglu *et al*, 1997; Bahar and Rader, 2005) to play the critical

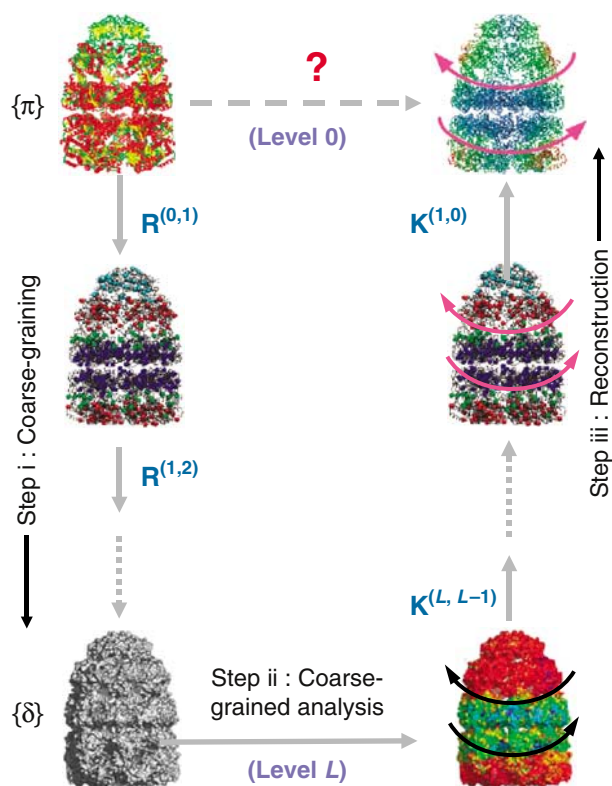


Figure 2 Hierarchical network decomposition overview. Step i: mapping of the structure to its optimal reduced level representation (coarse-graining); step ii: structural/dynamic analysis—for example, GNM analysis of collective dynamics (Bahar *et al.*, 1997; Haliloglu *et al.*, 1997)—in the reduced space; and step iii: reconstruction of the detailed structure dynamics. The communication/couplings of residues at a given level are assumed to obey a Markov propagation process consistent with the distribution of atom–atom contacts in the original structure. Steps i and iii are achieved by two sets of operators, \mathbf{R} for model reduction and \mathbf{K} for model reconstruction (Chennubhotla and Jepsen, 2005) explained in Materials and methods. Several models of intermediate complexity (not shown) are usually generated between the highest and lowest levels. \mathbf{R} and \mathbf{K} at each level ensure that similar stochastic characteristics (signal propagation probabilities and stationary distribution of communication) are retained between successive levels of the hierarchy. In particular, the reduction operator $\mathbf{R}^{(l,l+1)}$ propagates residue information from level l to $l+1$. Successive multiplication of such transformation matrices, as in $\mathbf{R}^{(0,L)} = \prod_{l=0}^{L-1} \mathbf{R}^{(l,l+1)}$, ensures the passage of information from the original, or the highest, resolution representation (level 0) to the most reduced level (level L) of the hierarchy. The arrows on the right illustrate the most cooperative motion (counter-rotation of the two rings) predicted by elastic network model analysis of GroEL–GroES(ADP)₇ (Keskin *et al.*, 2002).

role of messengers in the transmission of allosteric signals, as will be demonstrated below.

Markov process of network communication

A *discrete-time, discrete-state Markov* process is defined by setting the communication probability between residue pairs to be a function of their interaction strength, also called *affinity*. In particular, the $\{ij\}$ th element of the affinity matrix $\mathbf{A} = \{a_{ij}\}$ is defined as

$$a_{ij} = \frac{N_{ij}}{\sqrt{N_i N_j}} \quad (1)$$

where N_{ij} is the total number of *atom–atom* contacts made between residues v_i and v_j based on a cutoff distance of $r_c = 4.5 \text{ \AA}$ and (N_i, N_j) are the total numbers of heavy atoms in the individual residues (v_i, v_j) . The network may be alternatively viewed as a mass-spring system where pairs of (interacting) residues are connected by elastic springs with force constant $a_{ij} = a_{ji}$. The self-contact a_{ii} is similarly defined, but all bonded pairs are excluded. This representation captures to a first approximation the strong (weak) interactions expected to take place between residue pairs with large (small) numbers of atom–atom contacts, and removes biases due to size effects.

Using a measure of the local interaction density at each residue, given by $d_j = \sum_{i=1}^n a_{ij} = \sum_{j=1}^n a_{ji}$ (where n is total number of residues in the network), which in matrix form is $\mathbf{D} = \text{diag}\{d_j\}$, we define $m_{ij} = d_j^{-1} a_{ij}$ as the conditional probability of transmitting information to residue v_i in *one time step* given that the signal is initially positioned at residue v_j . Note, d_j serves as a normalizing factor to ensure $\sum_{i=1}^n m_{ij} = 1$. The conditional probability matrix $\mathbf{M} = \{m_{ij}\}$, also called the Markov transition matrix, given by

$$\mathbf{M} = \mathbf{A}\mathbf{D}^{-1} \quad (2)$$

fully defines the stochastics of signal diffusion over the network of residues.

Suppose the probability of initiating the Markov propagation process at node j is p_j^0 . Then, the probability of reaching residue v_i in one time step is $m_{ij} p_j^0$. In matrix notation, the probability of ending up on any of the residues $\mathbf{v} = [v_1, v_2, \dots, v_n]$ after one time step is given by the distribution $\mathbf{p}^1 = \mathbf{M}\mathbf{p}^0$, where $\mathbf{p}^k = [p_1^k, \dots, p_n^k]$. Clearly, this process can be iterated, so that after β steps we have

$$\mathbf{p}^\beta = \mathbf{M}^\beta \mathbf{p}^0 \quad (3)$$

Assume there is a path connecting every pair of residues in the network. Then, as $\beta \rightarrow \infty$, the Markov chain \mathbf{p}^β approaches a unique *stationary* distribution π , the elements of which are given by $\pi_i = d_i / \sum_{k=1}^n d_k$. Whereas the evolution of the diffusion process is a function of the starting distribution, the stationary distribution is invariant to the details of initiation (Norris, 1997).

Hierarchical model reduction based on Markov stochastics

For a clear understanding of the most probable mechanisms of signal propagation across the structure, we mapped the original structure onto successively lower resolution network models, while maintaining its stochastic characteristics (Figure 2). To build a hierarchy of intermediate resolution networks, we devise two sets of new operators: \mathbf{R} for model reduction and \mathbf{K} for model expansion/reconstruction (see Materials and methods). The $\{ij\}$ th element $\mathbf{R}_{ij}^{(0,L)}$ describes the probabilistic participation of residue v_i in cluster j at hierarchical level L . Alternatively, $\mathbf{R}_{ij}^{(0,L)}$ may be viewed as a measure of the ownership of residue v_i by cluster j generated at level L . The maximal ownership of a given residue v_i is defined as

$$\mathbf{R}_{i,\max}^{(0,L)} \equiv \max(\mathbf{R}_{ik}^{(0,L)}) \quad (4)$$

for $1 \leq k \leq c(L)$, where $c(L)$ is the total number of clusters at level L . $R_{i,\max}^{(0,L)}$ provides a measure of the involvement of residue v_i in the cluster that maximally owns it. In particular, this property reflects the potential of a residue for serving as a *hub* in any cluster derived at level L .

We also define the entropy $S_i^{(0,L)}$ of residue v_i as

$$S_i^{(0,L)} \equiv - \sum_k R_{ik}^{(0,L)} \ln R_{ik}^{(0,L)} \quad (5)$$

where the summation is performed over all clusters. $S_i^{(0,L)}$ provides a measure of the communication ability of residue v_i between clusters at level L . High entropy values refer to residues more or less uniformly shared by multiple clusters, thus playing the key role of a *messenger* in transmitting signals/perturbations. These are also referred to as sites having a high allosteric potential.

Soft partitioning of structure into stochastically coherent clusters

The GroEL–GroES(ADP)₇ structure (Xu *et al*, 1997) of $n=8015$ residues/nodes was mapped into a series of hierarchically reduced representations, comprised of $c(L)=1316, 483, 133, 35$ and 21 nodes for $L=1-5$, using the Markov chain propagation theory described in Materials and methods.

Each node at a given reduced level is a *coherent cluster* that provides a *soft partitioning* of the original structure, with regard to its communication stochastics, over increasingly large distance ranges. Thus, in contrast to the deterministic assignment of one-node-per-residue in the original network (level ‘0’), each cluster probabilistically contains a subset of residues, quantitatively expressed by its ownership distribution.

We focus on reduced level 4 ($c=35$) as the highest level that provides new insights into Markov propagation stochastics (level 5 practically partitions the complex into its 21 monomeric chains). Five sets (I–V) of seven symmetrically related clusters (Figure 3A) are obtained, centered near the GroES chains (clusters 1–7), the domains A–I (8–14) and E (15–21) of the *cis* ring and the domains E–I1 (22–28) and A–I2 (29–35) of the *trans* ring. Interestingly, the GroEL subunits are each partitioned into two clusters, although they comprise three structural domains E, I and A. Domain-I residues play a pivotal role, being integrated into E- or A-centered clusters, and their type and strength of participation in these clusters differ in the *cis* and *trans* rings. Panel B in Figure 3 illustrates the probabilistic participation of residues in two example clusters (encircled in panel A). The color code from red to blue indicates the gradually decreasing strength/probability of being owned by the particular clusters. A more quantitative analysis of these ownerships and comparison with experimental data are presented next.

Intra- and inter-subunit couplings and biological implications

Five ownership distributions (labeled 1–7, 11, 18, 25 and 32 in Figure 3D; colored curves) are displayed, representative of each respective type (I–V) of clusters (Table I). The chain identifiers (A–G for *cis* subunits, H–N for *trans*

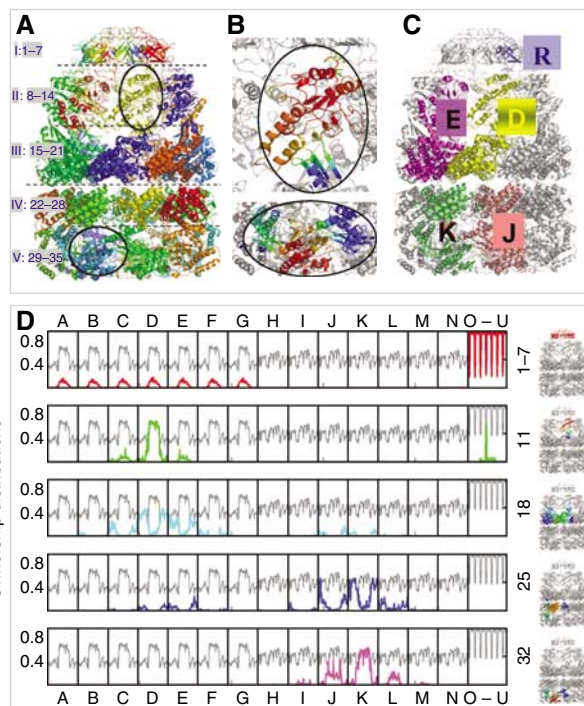


Figure 3 Soft partitioning of the chaperonin complex into stochastically coherent clusters. A total of 35 clusters are identified at reduced level 4, each shown by a different color in (A). Owing to the seven-fold cylindrical symmetry, five distinct types of clusters are observed: clusters (I) 1–7 centered on the GroES monomers, (II) 8–14 centered on AI domains of the *cis* ring subunits, (III) 15–21 around the E-domain of *cis* ring subunits, (IV) 22–28 near the E–I domains of *trans* ring subunits and (V) 29–35 near A–I domains of *trans* ring subunits. (B) displays the *soft* participation of residues in two example clusters encircled in panel A, clusters 11 (top) and 32 (bottom) respectively, by ribbon diagrams, color-coded red–orange–yellow–green–cyan in the order of decreasing probabilistic participation. Results are valid for all cylindrically related seven subunits along the heptameric rings, but for illustration we focus on chains D (yellow) and E (magenta) on *cis* ring, J (pink) and K (green) on *trans* ring and R (blue) on GroES, in (C). (D) shows ownership distributions (curves in color) for representative clusters of different types, numbered 1–7, 11, 18, 25 and 32, with the associated clusters shown in color on the ribbon diagrams to the right. The labels on the abscissa indicate the chain identities: A–G on *cis* ring, H–N on *trans* ring and O–U on GroES cap. The gray curve in each panel shows the maximal responsibility curve deduced from the maxima of all ownership curves. The portions of the ownership curves, which overlap with the maximal responsibility curve, define the hard clusters displayed in panel A.

subunits and O–U for GroES chains) adopted in the PDB (Berman *et al*, 2000) are shown along the abscissa. We focus on the subunits that are predominantly owned by the five representative clusters, that is, chains D, E, K, J and R, the locations of which on the 3-d structure are shown in Figure 3C. The results are valid for all seven symmetrically related clusters/subunits. The gray curve in each panel depicts the maximal responsibility $R_{i,\max}^{(0,L)}$ (equation (4)), assumed by residue v_i in the overall communication stochastics of the network.

The ownerships of individual clusters reveal several functional features. Below is a summary of results and relevant experimental data by various groups (see also Table I and Supplementary Table S1 (Supplementary information)).

Table I Distribution of residues in representative clusters

	Cap		Cis		Trans	
	Clusters 1–7	Cluster 11	Cluster 18	Cluster 25	Cluster 32	
Chain R Chain C	ALL except E18–A33	E18–A33	E1: A2–V6 E2: D523–P525			
Chain D		A: ALL I1: ALL except *S139–D140 I2: ALL except A384–V387, A406–G410	E1: ALL except A2–V6, V38–I49 E2: ALL except D523–P525 I1: S139–D140 I2: A406–G410			
Chain E			E1: V38–I49 I2: A384–V387			
Chain K				E1: ALL except R36–K51 E2: ALL I1: C138–E164 I2: K393–G410	A: ALL I1: A165–E178, Q184–G192 I2: V376–K380	
Chain J				E1: R36–K51	I1: D179–L183 I2: V381–K392 A: V268–K272	

See Figure 4 for the position of the clusters (in panel A) and GroEL–GroES chains (in panel D).

Key role played by GroES residues Glu18–Ala33 in achieving the communication between the *cis* ring and the co-chaperonin

This segment coincides with the exceptionally long ‘mobile loop’ that has been pointed out to serve as an allosteric modulator of the GroEL/substrate affinity (Landry *et al.*, 1993) and chaperonin cycle speed (Shewmaker *et al.*, 2001). It undergoes a transition from disordered to ordered (β -hairpin) form concomitant with binding to the A-domain of GroEL subunits (Shewmaker *et al.*, 2004). Site-directed mutagenesis experiments also support its key role in chaperone function (Landry *et al.*, 1993; Hohfeld and Hartl, 1994; Kovalenko *et al.*, 1994; Richardson and Georgopoulos, 1999; Richardson *et al.*, 1999, 2001). Our analysis demonstrates that this GroES loop is anchored into the apical domains of the adjoining *cis* ring subunits. This feature follows from the examination of the ownership curve for cluster 11 in Figure 3D. This cluster owns the entire A- and I-domains of chain D, except for a few residues in its I-domain (Ser139–Asp140, Ala384–Val387 and Ala406–Gly410). Remarkably, this cluster embodies the loop residues Glu18–Ala33 (peak at the O–U portion of the curve) that (chemically) belong to the neighboring co-chaperonin chain R. Figure 4A illustrates the mediating role of this loop (colored orange) between the apical domain of chain D (yellow) and the R chain of the cap (blue).

Positive intra-ring cooperativity imparted by crosstalks between the equatorial domains of adjacent subunits

Let us first examine cluster 18. The corresponding ownership curve in Figure 3D shows that this cluster is centered around the E-domain of subunit D. It embodies the entire E-domain except for the N- and C-termini (Ala2–Val6 and Asp523–

Pro525) and the E1 residues Val38–Ile49. We note that Val38–Ile49 form two anti-parallel β -strands connected by a loop that extends toward the neighboring subunit C and indeed belong to the adjoining cluster centered at subunit C, whereas the same stretch of residues on subunit E is integrated into the cluster 18 centered on subunit D (Figure 4B). Thus, viewed from the cap, all seven clusters of type III recruit this particular segment from their *clockwise* neighbor into their own cluster. Figure 4B shows this subunit E segment (orange) at the interface between subunits D (yellow) and E (magenta).

In the case of *trans* ring, on the other hand, a close examination of cluster 25 ownership reveals that inter-subunit coupling is achieved by the segment Arg36–Lys51 on the equatorial domain. Figure 4D illustrates how this particular segment of subunit J establishes the bridge between subunits J (pink) and K (green). This type of insertion of segments of 10–15 residues into neighboring stochastically coherent clusters suggests a functional mechanism for ensuring inter-subunit, intra-ring communication. The repetition of the same type of coupling across all the seven subunits is consistent with the known positive intra-ring cooperativity.

Intra-ring couplings exhibit opposite rotational directions in the *cis* and *trans* rings

Clusters 25 and 32 on the *trans* ring are comparable to the respective clusters 18 and 11 on the *cis* ring, in that they are dominated by the respective domains E and A of their subunits. The counterpart of chain D becomes chain K (green in Figure 3C), and its most closely communicating neighbor is chain J (pink), which replaces E. The counterpart of Figure 4B becomes Figure 4D. Comparing these two panels, an immediate observation is that the *trans* ring clusters recruit

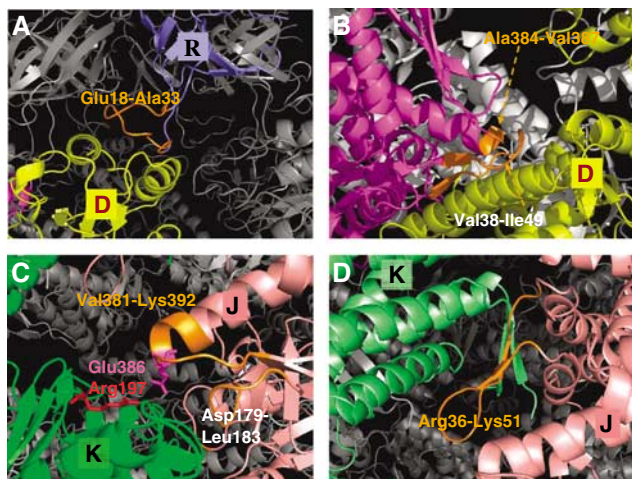


Figure 4 A closer view of intra- and inter-subunit couplings at the interface of the clusters. Results are shown for the representative chains D (yellow) and E (magenta) on *cis* ring, J (pink) and K (green) on *trans* ring and R (blue) on GroES. The chain segments that establish the communication between clusters are colored orange. **(A)** Residues Glu18–Ala33 in the mobile loop (orange) of GroES chain R integrated into the cluster centered at the A-domain of chain D establish the communication between *cis* ring and co-chaperonin. **(B)** Positive intra-ring cooperativity imparted by the coupling of chain E residues, Val38–Ile49 and Ala384–Val387 shown in orange, into cluster 18 dominated by chain D. **(C)** Inter-subunit couplings at *trans* ring A-domains. Cluster 32 embodies the A-domain of chain K, but also captures a few residues (Val381–Lys392, Asp179–Leu183; shown in orange) from chain J. **(D)** Cluster 25 is centered on the E-domain of chain K on *trans* ring. Note that this cluster engages E1 residues Arg36–Lys51 from chain J. Negative cooperativity between the two rings can be compared by comparing panels B and D, both corresponding to the E-domains of the respective *cis* and *trans* rings. The residues serving as messengers (orange) between the subunits belong to either clockwise (panel B) or counterclockwise (panel D) neighbors, as viewed from the cap, that is, the two rings have opposite rotational direction of inter-subunit couplings. The distribution of different chain residues in the examined representative clusters is listed in Table I.

segments (colored orange) from their counterclockwise neighbors when viewed from the cap, as opposed to the engagement of clockwise neighbors by *cis* ring subunits. We note that the two rings exhibit comparable contact topology and communication stochastics, when examined in isolation. However, their particular back-to-back arrangement within the quaternary structure results in opposite angular directions of communication around the cylindrical axis of symmetry. This anti-correlation in the communication directions of the two rings is suggestive of an intrinsic, structure-induced tendency to convey signals in opposite directions, which seems consistent with the well-known negative cooperativity between the two rings (Yifrach and Horovitz, 1995).

Coherence of *trans* ring assisted by inter-subunit communication between apical domains

Clusters 32 and 11 are both centered on the A-domains of the respective chains K and D. A striking difference between them is, however, the close involvement of an intra-ring neighbor J in the former, whereas the latter is confined to the single chain D. In other words, a coupling between adjacent subunits on *trans* ring is ensured by the apical-domain-centered clusters,

whereas their counterparts in the *cis* ring do not entail any intra-ring communication, but rather a coupling to the cap chain R. Two segments from I-domains of chain J are recruited by chain K: Asp179–Leu183 and Val381–Lys392 (Figure 4C).

This type of I–A domain inter-subunit coupling operating exclusively in *trans* ring may fulfill a functional requirement, in that the *trans* ring, when compared to *cis*, lacks the stabilizing effect of a bound co-chaperonin cap. Among the two stretches of residues that achieve this stabilizing effect, we note, in particular, that Glu386 on chain J forms a salt bridge with Arg197 on chain K (Figure 4C). This interaction has been pointed out to be crucially important for interlocking the seven subunits in their ‘closed’ form assumed in the *trans* ring; in the ‘open’ form of the subunits (i.e. *cis* ring), on the other hand, these salt bridges are broken in concert with the conformational changes that accommodate the binding of ATP and co-chaperonin GroES (Braig *et al*, 1994; Yifrach and Horovitz, 1998; Ma *et al*, 2000).

Key structural elements mediating allosteric interactions

The present analysis permits us to identify two classes of key residues: those serving as *hubs* in the individual clusters at a reduced level representation, and those mediating the communication between these clusters.

Hubs are distinguished by peaks in the maximal responsibility R_i^{\max} distributions, shown by the (identical) gray curves in Figure 3D, also reproduced in Figure 5A. The hubs identified on the *cis* ring are Ile333–Asp334, Lys321–Val323, Glu214–Ser217. Interestingly, the hubs coincide with β -strands termini or β -hairpins, or helices, suggesting a role for secondary structures in mediating allosteric communication. Val323 was also identified as an important site for allosteric communication in the study of Kass and Horovitz (2002). We note that no hub center is located on the intermediate domains. The I-domains indeed serve as regions for communication (messengers), rather than collection (hubs), of signals. As to the *trans* ring, Arg350–Glu355 in the apical domains and Val128–Glu129 serve as hub centers. Finally, we note that the GroES chains yield very high peaks in the R_i^{\max} distributions (Figure 3D). The corresponding hubs are found to be Glu50–Glu53.

The residues in the second class are shared by multiple clusters, and take on the job of *messengers* between these clusters. They are distinguished by their high allosteric potential, that is, their high ‘entropy’ values, $S_i^{(0,L)}$, deduced from their stochastic participation in different clusters (equation (5)). Both the red curve in Figure 5A and B and the color-coded ribbon diagram in panel C (colored from red-to-blue with decreasing entropy) reveal that the E-domains on the *cis* ring possess the highest entropies in the GroEL–GroES complex. The caps are distinguished by their low entropies.

In terms of the ability to communicate information, the predicted entropies point to the propensity of the *cis* ring E-domains to ‘broadcast’ information to all other structural parts, and in particular to transmit allosteric signals across the ring–ring interface. The highest entropy residues presently identified (peaks in Figure 5B) are Glu461–Val464, and Thr30–Lys34 in both *cis* and *trans* rings. Strikingly, the mutant E461K

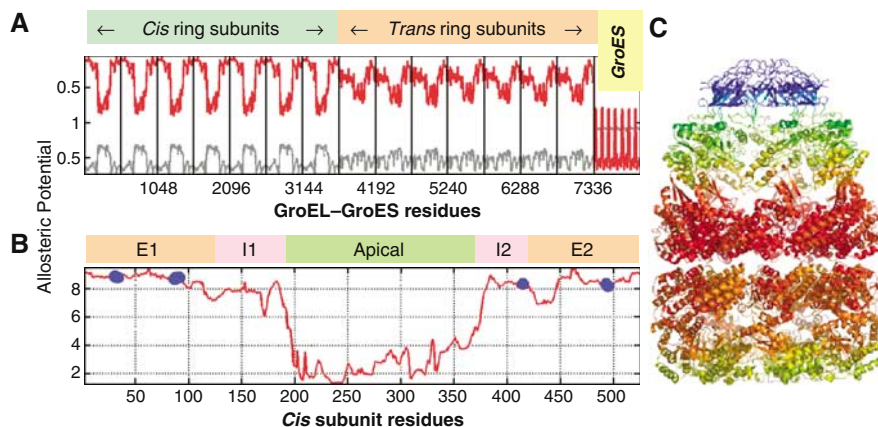


Figure 5 Regions of high broadcasting ability. **(A)** Residues acting as *hubs* lie on the peaks of maximal responsibility curve shown in gray, whereas residues shared by multiple clusters take on the job of *messengers*. They have high entropy values (red curve). **(B)** A detailed representation of the entropy curve for subunit D in the *cis* ring. Blue circles represent residues making at least two atom-atom contacts with the ADPs in the GroEL-GroES(ADP)₇ complex. All amino acids in/near the nucleotide-binding pocket are located in this high entropy region. **(C)** Entropy values as a color-coded ribbon diagram. Code: red-orange-yellow-green-blue, in the order of decreasing entropy. Equatorial domains of the *cis* ring subunits possess the highest entropy values, whereas the cap residues are distinguished by their low entropies.

has been shown in a recent study by Saibil and co-workers (Sewell *et al*, 2004) to cause defective folding. This behavior has been explained by the fact that the signal induced by ATP binding to the *trans* ring could not be transmitted across the ring-ring interface, and consequently the *cis* ring could not release its bound GroES. This observation lends support to the role of these highest entropy residues in ensuring the communication between the two rings. Finally, we note that ATP-binding residues generally exhibit high entropies, consistent with the requirement to propagate signals to distal regions. The filled circles in Figure 5B refer to the amino acids Pro33, Thr90, Gly88, Ile493, Leu31, Gly32, Thr91, Asp495, Gly415 and Asp87 that coordinate ADPs in the examined structure.

Proposed path(s) of communication between nucleotide- and co-chaperonin-binding sites

Among the residues located in the nucleotide-binding site, two highly conserved residues are distinguished by their large number (≥ 15) of atom-atom contacts with ADPs: Thr90 and Pro33. We focused on these two residues as initiation loci for signal transmission, and examined how the allosteric communication with the co-chaperonin-binding site is established. The GroES residues Ile25 and Gly24, reported in previous work to be conserved (Stan *et al*, 2003), were found here to act as communication cores (highest R_i^{\max}) within the loop residues. So we explored the maximum likelihood pathways originating from Thr90/Pro33 in the *trans* ring and ending at GroES-Ile25/Gly24, by using an algorithm similar to the shortest-path algorithm of Dijkstra's (Cormen *et al*, 1990). In particular, we define the *distance* between two residues v_i and v_j in the network as $-\log(m_{ij})$; so the higher the communication probability, the lower the distance between nodes, and these distances in turn are taken into consideration in evaluating the maximum-likelihood path.

Figure 6A displays the resulting two maximum likelihood pathways. The first, labeled (I), runs between Thr90 (subunit

K) and Ile25 (subunit R) following the scheme **T90** → V94 → N97 → **T101** → K105 → A109 on subunit K, succeeded by K105 → **E102** → I99 → A508 → Q505 → **R501** → **E409** → **E408** → R404 → V174 → **A370** → **K371** → **M193** → I332 → I220 → F219 → V240 → A241 on subunit D and ending at **I25** → **G24** on the cap chain R. The shortest path originating from Pro33 (labeled (II) in Figure 6A), on the other hand, is **P33** → **G32** → **I454** → R452 → on chain K succeeded by **E461** → E460 → C458 → **K34** → **P33** → **N153** → S154 → **D155** → V158 → L161 → L187 → V189 → V190 → Q194 → F195 → **R197** → **G198** → **Y199** → P202 → **Y203** on chain E and I305 → G306 → K311 → **E310** → M233 → L234 on chain D, and finally ending at **G23** → **G24** on the cap chain R. Interestingly, these two paths, both originating from the same ATP-binding region on subunit K in the *trans* ring evolve through different subunits (D and E) on the *cis* ring to merge at the same target site on the co-chaperonin mobile loop.

Several residues on these pathways exhibit interesting features: the boldfaced ones are conserved within the Hsp60/GroEL family (Fenton *et al*, 1994; Stan *et al*, 2003); and those written in italic are distinguished by their high communication entropies. We note that the intra-subunit interaction between residues **E409** and **R501** has been pointed to be implicated in the allosteric mechanism of GroEL (Aharoni and Horovitz, 1997). We also note that D155 has been pointed out to disrupt the intra-ring cooperativity of the ATP-bound ring (Danziger *et al*, 2003; Horovitz and Willison, 2005). Inter-ring cooperativity was observed by Aharoni and Horovitz (1996) to be disrupted in the GroEL double mutant (R13G, A126V), while the double mutant was functional both *in vivo* and *in vitro* (Fenton *et al*, 1994). These residues could not be observed in the presently examined maximum likelihood pathways.

The on-pathway residues at the interface between the *cis* and *trans* rings (A109, K105, R452, **E461**) should be expected to play a key role in assisting the communication between the two rings. We note among them Glu461 in *cis* subunit E that is receiving signal from R452 on *trans* subunit K. Note that Glu461 is the residue whose substitution by lysine has been

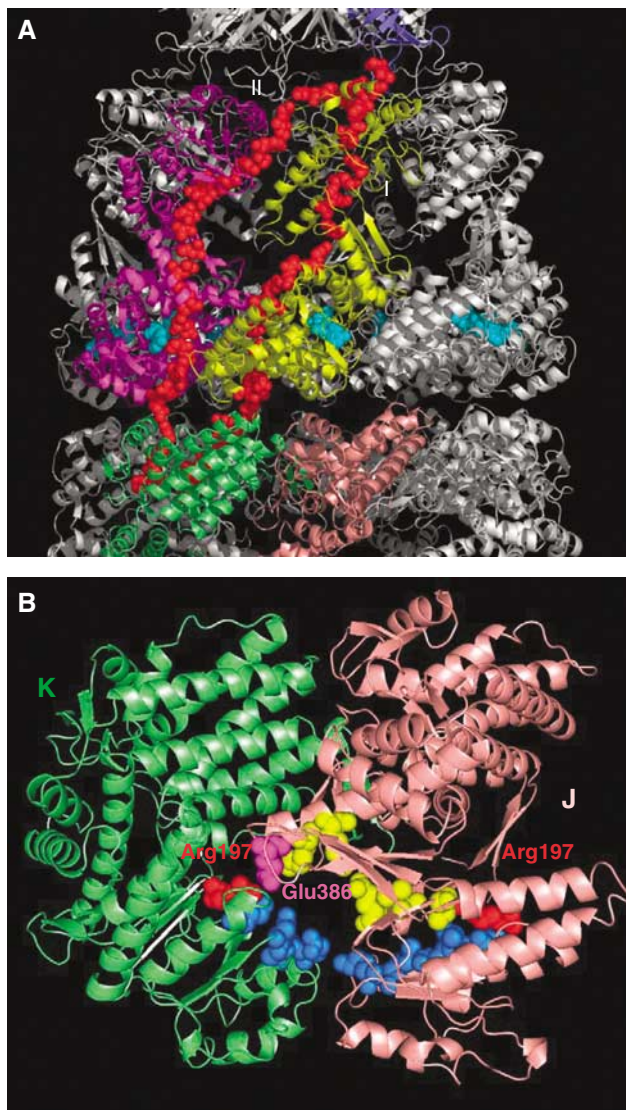
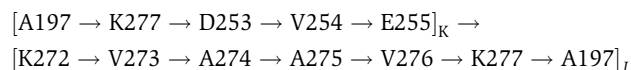


Figure 6 Inter- and intra-ring communication pathways. **(A)** Two maximum likelihood pathways (red spheres), labeled I and II, originating from residues Thr90 and Pro33 respectively, on subunit K near the nucleotide-binding site, and ending in residue Gly24 on the GroES mobile loop. The ADP molecule near subunit D is shown in cyan. **(B)** Maximum likelihood pathway originating from Arg197 (red) on subunit K and ending in Arg197 (red) on subunit J. The pathway is shown in yellow, achieved readily through the salt bridge Arg197-Glu386. Residue Glu386 on subunit J is shown in magenta. Also shown in blue is the pathway computed for the mutant R197A. The latter involves four additional residues in subunit K.

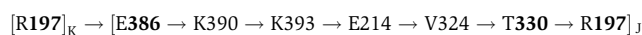
shown in a recent work by Saibil and co-workers (Sewell *et al.*, 2004) to impede the release of the co-chaperonin (bound to the *cis* ring). This long-range effect has been shown to be owing to the disruption of the inter-ring transmission of the signal from ATP-binding site on the *trans* ring, caused by the of the originally out-of-register alignment of subunits across the rings (K, D and E in the present case) into in-register alignment (Sewell *et al.*, 2004). The present analysis demonstrates that Glu461 (on *cis* subunit E) is indeed on the most probable pathway, and significantly, it forms an *intermolecular* salt

bridge (with R452 on *trans* subunit K) at the interface between the two rings.

Additionally, the above analysis focuses on inter-ring communication. Of interest is to assess pathways of intra-ring communication as well (Figure 6). We focus in particular on R197, a conserved residue whose mutation to alanine has been pointed out in previous work to elicit allosteric changes (White *et al.*, 1997). As pointed out above, Arg197 participates in the small set of residues (see Table I and Supplementary Table S1 (Supplementary information)) that establish the inter-subunit communication in the *trans* ring, by way of forming a salt bridge with Glu386. In order to assess the role of Arg197 in ensuring/facilitating the intra-ring communication, we explored the maximum likelihood pathways originating from Arg197 on *trans* ring and ending, again, on Arg197 in neighboring subunit in the same ring (an effect that propagates across all seven subunits in the ring). In Figure 6B, residue R197 is shown in red on subunits K and J. Calculations were performed both for the wild-type protein and the R197A mutant generated *in silico*. We obtained the path



for the mutant, as opposed to the path



for the original structure. Here the subscripts refer to the subunits involved, and conserved residues (Fenton *et al.*, 1994) are shown in boldface. Clearly, the wild-type sequence samples a much shorter pathway. The passage across the two subunits is readily achieved through the salt bridge R197-E386 at the initiation step. In Figure 6B, residue Glu386 is shown in magenta on subunit J. A cascade of charge-charge interactions is implicated in this pathway, suggesting an effective signal transfer mechanism. The most probable path undertaken by the mutant R197A, on the other hand, involves four additional residues in subunit K, before reaching the neighboring subunit J. In particular, the interaction with the conserved residue K277 seems to favor this longer pathway.

Correlation with collective dynamics: physical role of hubs and messengers

Significant progress has been made in recent years in improving our understanding of the collective dynamics of biomolecular systems in relation to their biological functions and interactions, using normal mode analyses with coarse-grained models (Bahar and Rader, 2005; Ma, 2005). The GNM (Bahar *et al.*, 1997; Haliloglu *et al.*, 1997) is such a model widely resorted to in recent years. Based on statistical mechanical theory of macromolecular networks (Flory, 1976), the GNM provides a rapid assessment of the key mechanical sites (e.g., hinges) that coordinate global (domain) motions (see e.g. Yang and Bahar (2005) for a systematic analysis of enzyme dynamics). The application of the GNM and its extensions to GroEL-GroES (Keskin *et al.*, 2002) has shown that concerted counter-rotations of the *cis* and *trans* rings are the most probable collective motions intrinsically favored by the overall architecture, in accord with the motions deduced from the

comparison of X-ray or cryo-EM structures determined in different states.

The approach taken by the GNM analysis is to deduce the spectrum of normal modes from the eigenvalue decomposition of the Kirchhoff matrix of inter-residue contacts, Γ , specific to the examined structure/network topology. A bridge between signal propagation dynamics presented here (based on information theory, graph theoretic methods and Markovian stochastics) and the GNM dynamics (based on fundamental concepts of solid state physics and macromolecular statistical mechanics) is the relationship

$$\Gamma = \mathbf{D} - \mathbf{A} \quad (6)$$

Equation (6) identically holds provided that the nonzero off-diagonal elements of \mathbf{A} and Γ are defined as $a_{ij} = \Gamma_{ij} = 1$ in line with the original GNM, or as $a_{ij} = \Gamma_{ij} = N_{ij} / \sqrt{(N_i N_j)}$ after the presently defined affinity matrix (equation (1)). The latter provides a more detailed description of inter-residue interactions than the original GNM, as it incorporates information on the density of atom-atom contacts in addition to the information on network connectivity. Γ is also referred to as the combinatorial Laplacian in graph theory (Chung, 1997).

The equilibrium dynamics of the network is fully defined by Γ ; in particular the mean-square fluctuations of residues are readily computed from the relation $\Delta \mathbf{r}_i^T \Delta \mathbf{r}_i = \frac{3k_B T}{\gamma} [\Gamma^{-1}]_{ii}$ where $[\Gamma^{-1}]_{ii}$ designates the i th diagonal element of the inverse of Γ , k_B is the Boltzmann factor, T is the temperature and γ is the spring constant that uniformly scales the amplitudes of fluctuations, without affecting their residue distributions (for a review see Chennubhotla *et al*, 2005).

We used the presently introduced Markov chain-based hierarchy to build reduced Kirchhoff matrices, $\tilde{\Gamma}$, at increasingly lower levels of resolution, ranging from $c=8015$ nodes at the full-residue representation to $c=21$ nodes at level $L=5$, congruent with the $\tilde{\mathbf{A}}$ matrices derived at various hierarchical levels. We repeated the GNM analysis at successive levels to explore how well the original ($L=0$) fluctuation behavior is preserved upon mapping the structure to its lower resolution counterparts, performing the GNM analysis in the reduced spaces and reconstructing the fluctuation dynamics at the original level (see the scheme in Figure 2). We call this new approach the *hierarchical GNM* (see Chennubhotla and Bahar, 2006 and Supplementary information for more details). In addition to this ‘fidelity’ test, we also explored how the correlation between theoretically predicted mean-square fluctuations of residues and experimental data, X-ray crystallographic B -factors in this case, varies by adopting various levels of coarse-graining.

Figure 7A displays the comparison of the fluctuations of residues, $\langle \Delta \mathbf{r}_i^T \Delta \mathbf{r}_i \rangle$, obtained at various levels of Markov hierarchy with those indicated by the X-ray crystallographic B -factors (black curve) $B_i = (8\pi^2/3) \langle \Delta \mathbf{r}_i^T \Delta \mathbf{r}_i \rangle$ reported in the PDB (Xu *et al*, 1997). The theoretical fluctuations computed at various levels are hardly distinguishable and are all represented by the red curve. As shown in the inset, a correlation coefficient of 0.86 is achieved between experimental and theoretical fluctuation distributions after mapping the structure of 8015 residues into a network of 21 soft clusters. Thus, the fluctuation profile of residues is accurately predicted

despite a drastic reduction in the complexity of the examined network. Interestingly, a maximum correlation coefficient of 0.89 is obtained at an intermediate level of resolution, $c=133$, which may be attributed to an optimal elimination of noise in the data.

Next, we examine the role of hubs and messengers in the context of the collective dynamics of GroEL/GroES. It is also of interest to elucidate the type of involvement of residues distinguished here by their high allosteric potentials (maxima in entropy curve (red) in Figure 5A) in the most cooperative (global) modes of motion of the entire complex. A comparison of the entropy profiles of residues in the *cis* and *trans* ring subunits with their mobilities in the global mode of the chaperonin is presented in Figure 7B. The mobility profiles represent the distributions of square displacements in the lowest frequency mode, determined by eigenvalue decomposition of $\tilde{\Gamma}(L)$ for the entire complex. We note that the global modes are also verified to be maintained with a correlation coefficient of 0.99 at all levels $0 \leq L \leq 5$ of the hierarchy. The high mobility of the apical domain delimited at the A-I interfaces is revealed in Figure 7B, while the equatorial domains are rather stable. An immediate observation is the anti-correlation between the two sets of profiles in the top and bottom panels of Figure 7B. This property is more evident in panel C, where a decrease in allosteric potential is accompanied by an increase in mobility, in general. Thus, the minima in the global mode profiles, which have been shown in numerous applications to play a critical role (acting as hinges or anchors) in coordinating the functional dynamics of biomolecules (Bahar and Rader, 2005; Ma, 2005), act as messengers in the transmission of allosteric signals. Also shown in Figure 7C as blue dots are the locations of ATP-binding residues Leu31-Pro33, Asp87-Thr91, Gly415 and Asp495, exhibiting high entropies and low mobilities.

Conclusions

In the present study, we introduced a new methodology for elucidating the pathways of allosteric communication in large biomolecular systems. The approach is based on Markov propagation of information/perturbation over the network of interactions that stabilize a given structure. The approach permits us to simplify the original complex structure as a collection of ‘soft clusters’ at different levels of resolution. Each cluster probabilistically ‘owns’ groups of residues obeying coherent signal propagation stochastics. Those residues more or less equally ‘shared’ by adjoining clusters are instrumental in transmitting information across clusters and serve as *messengers*, whereas those almost completely owned by a given cluster serve as *hubs*. This description greatly simplifies our understanding of the dominant mechanisms and key elements that mediate the communication across distant regions in complex structures.

Using this new framework, we identified two pathways that are most likely to mediate the communication between the ATP- and co-chaperonin-binding sites (Figure 5D), comprising many conserved residues as well as those serving as hubs or detected in previous studies to be critical for chaperonin machinery. Two alternative mechanisms seem viable inasmuch as this coupling between E- and distal A-domains is

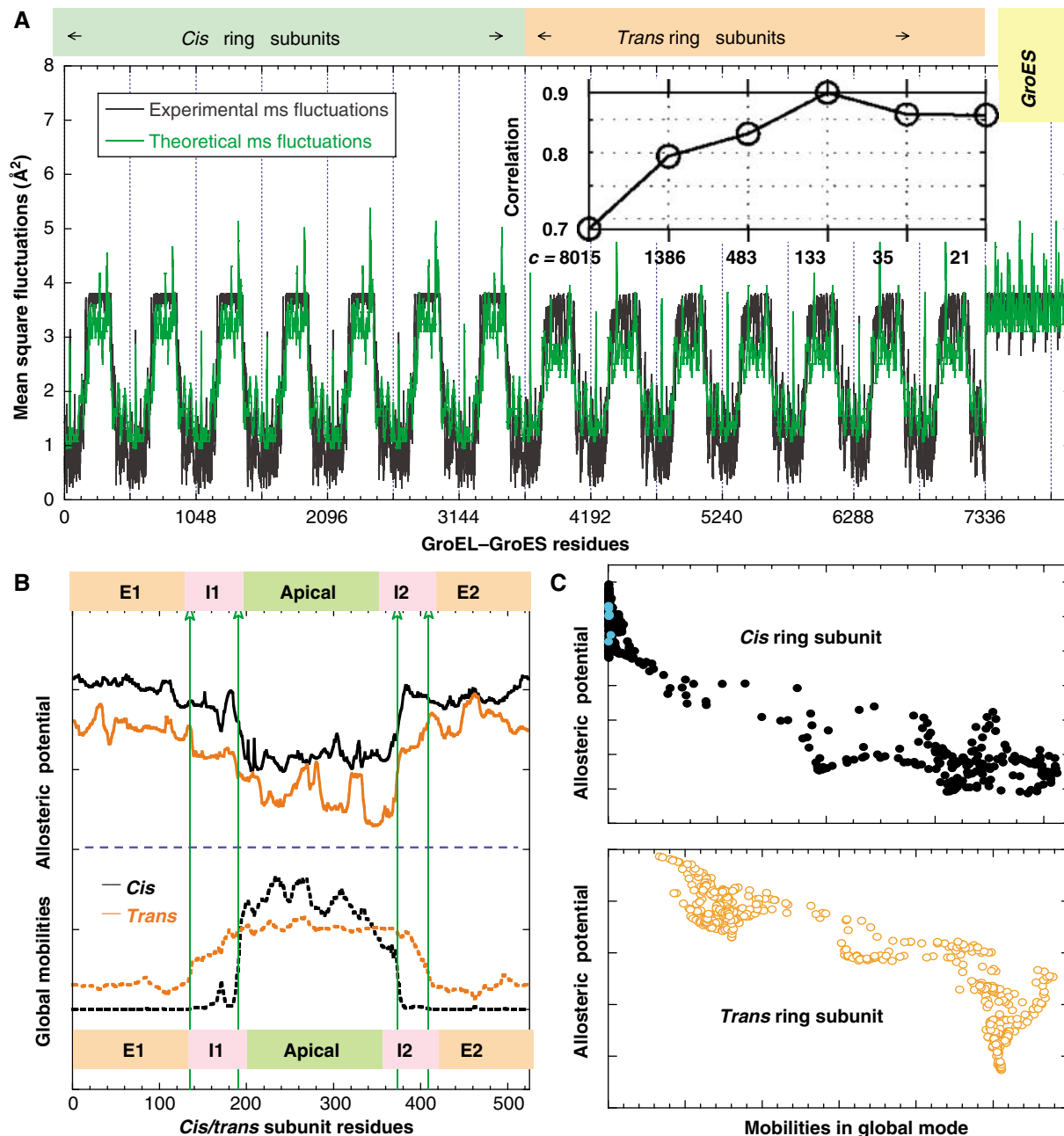


Figure 7 Collective dynamics and comparison with communication entropies. **(A)** Comparison of the experimental (black) and theoretical (green) distributions of mean-square fluctuations of residues. The theoretical curve is reconstructed from level 3 of the hierarchy. The inset shows the correlation coefficient between the theoretical B -factors derived from each level of the hierarchy (from full residue representation ($c=8015$) to the coarsest scale ($c=21$) and the experiment. Interestingly, the full residue representation (with 8015 residues) yields a correlation coefficient of 0.68 that is lower than coarse-grained representation. In particular, at level 3 ($c=133$), the correlation coefficient is 0.89. **(B)** Comparison of the communication potentials (entropies) of residues (upper panel) with their mobilities in the global mode (lower panel) for *trans* (orange) and *cis* (black) ring subunits. The communication entropies are computed using equation (5), at level $L=4$. Mobilities (normalized square displacements) are found from the lowest frequency GNM mode, almost identically reproduced at all levels of the hierarchy. **(C)** (Anti-)correlation between communication entropies and global mobilities, shown for the *cis* (top) and *trans* (bottom) ring subunits. The two sets of data yield respective correlation coefficients of 0.94 and 0.89, revealing a dual role, both mechanical stability and efficient signal propagation for a subset of residues distinguished by their restricted mobility. Also shown in panel C as blue dots are the locations of ATP-binding residues Leu31–Pro33, Asp87–Thr91, Gly415 and Asp495, exhibiting high entropies and low mobilities.

crucial for function. We note that in a recent ϕ -value analysis, Horovitz *et al* (2002) presented evidence for the existence of parallel pathways for the allosteric transition of the rings.

Our analysis highlights the pivotal role played by the I-domain in establishing intra-ring and inter-subunit commu-

nication. We observed inter-subunit I–A domain couplings that operate exclusively at *trans* ring. This may be a functional requirement, to ensure the coherence of the *trans* ring that lacks, compared to the *cis* ring, the stabilizing effect of the bound co-chaperonin cap. Among the residues that achieve

this stabilizing effect, we note, in particular, Glu386, which forms an inter-subunit salt bridge with Arg197, confirming previous results (see Table I and Supplementary Table S1 (Supplementary information)). We also studied the effect of the mutation R197A on intra-ring communication. R197 on the *trans* ring E-domain exhibits a strong preference to communicate with its salt-bridge-forming partner E386 on the nearest *cis* ring subunit in the wild-type structure, whereas the mutant R197A generated *in silico* preferentially interacts with K277 and D253 on the same (*trans*) ring, and reaches the *cis* ring via a substantially longer pathway.

A most striking observation is that inter-subunit couplings occur in opposite directions in *cis* and *trans* rings. Intriguingly, the information flows presently identified within the *cis* and *trans* rings have well-defined preferences for opposite rotations (clockwise versus counterclockwise, when viewed from the cap). For example, subunit D engages E in the *cis* ring, whereas K engages J in the *trans* ring (see Figure 4B and D). It should be noted, however, that this cooperativity is different in character than the one observed within rings. The intra-ring cooperativity is inherently ensured by the association of neighboring clusters via residues that are being shared, repeated across all seven subunits, consistent with a classical MWC cooperativity (Monod *et al.*, 1965; Horovitz and Willison, 2005). Such an integration of neighboring clusters is not observed across the interface between the two rings. The lack of a close cluster association at the interface, in contrast to that occurring within the rings, suggests that the stochastics of intra- and inter-ring couplings differ in their character and timescale, reminiscent of MWC type (intra-ring) interactions nested in KNF-like (Koshland *et al.*, 1966) inter-ring interactions (Horovitz and Willison, 2005).

The present analysis takes account of residue specificities in an approximate way (through the numbers of atom–atom contacts for each residue pair) and does not distinguish between strong or weak interactions. No electrostatic and solvent effects are included either. Despite the neglect of these physical features, the method offers a plausible model for information propagation between distinct functionally relevant sites of GroEL–GroES. The property rigorously taken into consideration here is the intricate topology of inter-residue contacts and local packing/interaction densities in the native state. The present analysis thus lends support to the dominant role of inter-residue contact topology in defining cooperative interaction mechanisms/pathways on a global scale, in accord with recent computational studies based on coarse-grained models (Bahar and Rader, 2005).

Identification of hubs and messengers raises implications for protein design. In the network communication paradigm, the equatorial domains of the *cis* ring emerge unambiguously as the regions with the highest propensity for ‘broadcasting’ the perturbations occurring in their domain. In particular, the E-domain residues Ser463 and Glu461 emerge as the amino acids with the highest allosteric potential (see equation (5); Figure 5). The critical role of Glu461 in establishing the negative inter-ring cooperativity is now established by the recent work of Saibil and co-workers (Sewell *et al.*, 2004), whereas that of Ser463 remains to be experimentally confirmed. The high broadcasting ability does not necessarily imply *efficient* transmission to a *given target* because the signal

can be dissipated in many directions. Yet, the observed involvement of messengers in maximum likelihood pathways may have other functional implications, for example, inducing other co-operative effects such as processing the substrate protein. We also examined the role of hubs and messengers in the context of collective dynamics of GroEL/GroES deduced from normal mode analysis. A significant property that emerges is that the minima in global mode profiles, which have been shown to play a critical role in coordinating functional dynamics of biomolecules, act as messengers in the transmission of allosteric signals. Automated identification of such residues serving as hubs and messengers in a given architecture, as proposed and illustrated here for GroEL–GroES, may help in efficient design and modification of protein structure and function.

Materials and methods

Deriving stationary distribution in the reduced model

We begin by expressing the stationary distribution $\pi = [\pi_1, \pi_2, \dots, \pi_n]$ as a probabilistic mixture of *latent* distributions,

$$\pi = \mathbf{K}\delta \quad (7)$$

where $\delta = [\delta_1, \delta_2, \dots, \delta_c]$ is an unknown stationary distribution in a reduced (c -dimensional) representation of the structure, $\mathbf{K} = \{K_{ij}\}$ is an $n \times c$ non-negative *kernel* matrix with elements K_{ij} and columns K_j being latent probability distributions that each sum to 1 and $c \ll n$. The kernel matrix acts as an *expansion* operator, mapping the low-dimensional distribution δ to a high-dimensional distribution π (see Figure 2). The high-dimensional distributions are referred to as high-resolution, or low-level, descriptions, and the low-dimensional distributions, as low-resolution, or high-level, descriptions.

We derive a maximum likelihood approximation for δ using an EM type algorithm (McLachlan and Basford, 1988). To this aim, we minimize the *Kullback–Liebler* distance measure (Kullback, 1959) between the two probability distributions π and $\mathbf{K}\delta$, given by

$$\mathcal{L} = - \sum_{i=1}^n \pi_i \ln \sum_{j=1}^c K_{ij} \delta_j + \sum_i \pi_i \ln \pi_i \quad (8)$$

A maximum likelihood estimate is obtained by minimizing

$$E = - \sum_{i=1}^n \pi_i \ln \sum_{j=1}^c K_{ij} \delta_j + \lambda \left(\sum_{j=1}^c \delta_j - 1 \right) \quad (9)$$

subject to the constraint $\sum_{j=1}^c \delta_j = 1$, ensured by the Lagrange multiplier λ . Setting the derivative of E with respect to δ_j to be zero, we obtain

$$\sum_{i=1}^n \frac{\pi_i K_{ij} \delta_j}{\sum_{k=1}^c K_{ik} \delta_k} = \lambda \delta_j \quad (10)$$

The contribution made by kernel j to a node i (or to its stationary probability π_i) is given by K_{ij} (or by the product $K_{ij} \delta_j$), and hence we can define an *ownership* of node i in the high-resolution representation by a node j in the low resolution as

$$R_{ij} = \frac{K_{ij} \delta_j}{\sum_{k=1}^c K_{ik} \delta_k} \quad (11)$$

We note that the mapping between the two resolutions is not deterministic, but probabilistic in the sense that $\sum_{j=1}^c R_{ij} = 1$.

Using this relation, and the equalities $\sum_{j=1}^c \delta_j = 1$ and $\sum_{i=1}^n \pi_i = 1$, summing over j in equation (10) gives $\lambda = 1$. This further leads to the stationary distribution δ at the coarse scale

$$\delta_j = \sum_{i=1}^n \pi_i R_{ij} \quad (12)$$

Following Bayes theorem, K_{ij} can be related to the updated δ values as

$$K_{ij} = \frac{R_{ij}\pi_i}{\delta_j} \quad (13)$$

In summary, the operators \mathbf{K} and \mathbf{R} and stationary distribution δ are computed using the following EM type procedure: (1) select an initial estimate for \mathbf{K} and δ (see Supplementary information for details); (2) *E-step*: compute ownership maps \mathbf{R} using equation (11); (3) *M-step*: estimate δ and update \mathbf{K} using equations (12) and (13) respectively; and finally, (4) repeat *E-* and *M-*steps until convergence.

Transition and affinity matrices at reduced levels

The Markov chain propagation at the reduced representation obeys the equation $\mathbf{q}^{k+1} = \tilde{\mathbf{M}}\mathbf{q}^k$, where \mathbf{q}^k is the coarse scale m -dimensional probability distribution after k steps of the random walk. We expand \mathbf{q}^k into the fine scale using $\mathbf{p}^k = \mathbf{K}\mathbf{q}^k$, and reduce \mathbf{p}^k back to the coarse scale by using the ownership value R_{ij} as in $q_i^{k+1} = \sum_{j=1}^n P_i^k R_{ij}$. Substituting equation (11) for ownerships, followed by the expression for \mathbf{p}^k , in the equation for q_i^{k+1} , we get

$$\tilde{\mathbf{M}} = \text{diag}(\delta)\mathbf{K}^T \text{diag}(\mathbf{K}\delta)^{-1}\mathbf{K} \quad (14)$$

Using the definition of $\tilde{\mathbf{M}}$, and the corresponding stationary distribution δ , we generate a symmetric affinity matrix $\tilde{\mathbf{A}}$ that describes the node-node interaction strength in the low-resolution network

$$\tilde{\mathbf{A}} = \tilde{\mathbf{M}} \text{diag}(\delta) \quad (15)$$

To summarize, we use the stationary distribution π and Markov transition matrix \mathbf{M} at the fine scale to derive a transition matrix $\tilde{\mathbf{M}}$, and its stationary distribution δ , at the coarse scale. It is obvious that this procedure can be repeated recursively to build a hierarchy of lower resolution network models.

Application to GroEL–GroES: interactions/affinities at different hierarchical levels

We examined the Markov process of inter-residue communication in the structure GroEL–GroES(ADP)₇, crystallographically characterized by Sigler and co-workers (Xu *et al.*, 1997), also known as the R' state of the bacterial chaperonin (Thirumalai and Lorimer, 2001). First, the inter-residue affinity matrix \mathbf{A} based on all atom–atom contacts (a total of $\approx 10^6$ interactions, based on an interaction range of 4.5 Å between all non-bonded heavy atoms) is constructed, which is then used in equation (2) to derive the fine-scale Markov transition matrix \mathbf{M} .

The kernel selection algorithm (Supplementary information) applied to \mathbf{M}^β ($\beta=4$) yields 1316 (reduced level 1) kernels. Using these kernels as an initialization, a recursive application of the EM procedure derives stationary distributions δ (equation (12)), updated expansion matrices \mathbf{K} (equation (13)), reduced level probability transition matrices $\tilde{\mathbf{M}}$ (equation (14)) and the corresponding residue interaction matrices $\tilde{\mathbf{A}}$ (equation (15)). The respective dimensions of $\tilde{\mathbf{A}}$ turn out to be 483 (level 2), 133 (level 3), 35 (level 4) and 21 (level 5). We note that the individual subunits of the GroEL–GroES are distinguished by their strong intra-subunit interactions, and a number of inter-subunit contacts are maintained at all levels, which presumably establish the communication across the protein at all levels. The dimension of the reduced model, c , is automatically defined during the kernel selection at each level of the hierarchy. The method thus avoids the arbitrary choices of sampling density and interaction cutoff distances at different hierarchical levels.

Supplementary information

Supplementary information is available at the *Molecular Systems Biology* website (www.nature.com/msb).

Acknowledgements

Support from NIH Grant #R33 GM068400-01A2 is gratefully acknowledged.

References

- Aharoni A, Horovitz A (1996) Inter-ring communication is disrupted in the GroEL mutant Arg13 → Gly; Ala126 → Val with known crystal structure. *J Mol Biol* **258**: 732–735
- Aharoni A, Horovitz A (1997) Detection of changes in pairwise interactions during allosteric transitions: coupling between local and global conformational changes in GroEL. *Proc Natl Acad Sci USA* **94**: 1698–1702
- Atilgan AR, Durell SR, Jernigan RL, Demirel MC, Keskin O, Bahar I (2001) Anisotropy of fluctuation dynamics of proteins with an elastic network model. *Biophys J* **80**: 505
- Bahar I, Rader AJ (2005) Coarse-grained normal mode analysis in structural biology. *Curr Opin Struct Biol* **15**: 1–7
- Bahar I, Erman B, Monnerie L (1994) Effect of molecular structures on local chain dynamics: analytical approaches and computational methods. *Adv Polym Sci* **116**: 151–206
- Bahar I, Atilgan AR, Erman B (1997) Direct evaluation of thermal fluctuations in protein using a single parameter harmonic potential. *Folding Des* **2**: 173–181
- Berman HM, Westbrook J, Feng Z, Gilliland G, Bhat TN, Weissig H, Shindyalov IN, Bourne PE (2000) The Protein Data Bank. *Nucleic Acids Res* **28**: 235–242
- Braig K, Otwinowski Z, Hegde R, Boisvert D, Joachimiak A, Horwich AL, Sigler PB (1994) The crystal structure of the bacterial chaperonin at 2.8 Å. *Nature* **371**: 578–586
- Changeux JP, Edelstein SJ (2005) Allosteric mechanisms of signal transduction. *Science* **308**: 1424–1428
- Chennubhotla C, Bahar I (2006) Markov models for hierarchical coarse-graining of large protein dynamics. *Lecture Notes in Computer Science* **3909**: 379–393
- Chennubhotla C, Jepsen A (2005) Hierarchical eigensolver for transition matrices in spectral methods. In LK Saul, Y Weiss & L Bottou (eds) *Adv. in Neural Information Processing Systems 17*, 273–280. Cambridge, MA: MIT Press
- Chennubhotla C, Rader AJ, Yang LW, Bahar I (2005) Elastic network models for understanding biomolecular machinery: from enzymes to supramolecular assemblies. *Phys Biol* **2**: S173–S180
- Chung FRK (1997) *Spectral Graph Theory*, CBMS Lectures. AM. Math. Soc., Providence, RI, USA
- Coifman RR, Lafon S, Lee AB, Maggioni M, Nadler B, Warner F, Zucker SW (2005) Geometric diffusion as a tool for harmonic analysis and structure definition of data, part I.: *Proc Natl Acad Sci USA* **102**: 21
- Cormen TH, Leiserson CE, Rivest RL (1990) *Introduction to Algorithms*. Cambridge, MA, USA: MIT Press
- Danziger O, Rivenzon-Segal D, Wolf S, Horovitz A (2003) Conversion of the allosteric transition of GroEL from concerted to sequential by the single mutation. *Proc Natl Acad Sci USA* **100**: 13797–13802
- de Groot BL, Vriend G, Berendsen HJC (1999) Conformational changes in the chaperonin GroEL: new insights into the allosteric mechanism. *J Mol Biol* **286**: 1241–1249
- Doruker P, Atilgan AR, Bahar I (2000) Dynamics of proteins predicted by molecular dynamics simulations and analytical approaches: application to α -amylase inhibitor. *Proteins* **40**: 512–524
- Fenton W, Kashi Y, Furtak K, Horwich A (1994) Residues in chaperonin GroEL required for polypeptide binding and release. *Nature* **371**: 614–619
- Flory PJ (1976) Statistical thermodynamics of random networks. *Proc Roy Soc London A* **351**: 351–378
- Haliloglu T, Bahar I, Erman B (1997) Gaussian dynamics of folded proteins. *Phys Rev Lett* **79**: 3090–3093
- Hinsen K (1998) Analysis of domain motions by approximate normal mode calculations. *Proteins* **33**: 417
- Hohfeld J, Hartl FU (1994) Role of the chaperonin cofactor hsp10 in protein folding and sorting in yeast mitochondria. *J Cell Biol* **126**: 305–315
- Horovitz A, Willison KR (2005) Allosteric regulation of chaperonins. *Curr Opin Struct Biol* **15**: 1–6

- Horovitz A, Amir A, Danziger O, Kafri G (2002) ϕ value analysis of heterogeneity in pathways of allosteric transitions: evidence for parallel pathways of ATP-induced conformational changes in GroEL ring. *Proc Natl Acad Sci USA* **99**: 14095–14097
- Kass I, Horovitz A (2002) Mapping pathways of allosteric communication in GroEL by analysis of correlated mutations. *Proteins* **48**: 611–617
- Keskin O, Bahar I, Flatow D, Covell DG, Jernigan RL (2002) Molecular mechanisms of chaperonin GroEL–GroES function. *Biochemistry* **41**: 491–501
- Koshland DE, Nemethy G, Filmer D (1966) Comparison of experimental binding data and theoretical models in proteins containing subunits. *Biochemistry* **5**: 365–385
- Kovalenko O, Yifrach O, Horovitz A (1994) Residue lysine-34 in GroES modulates allosteric transitions in GroEL. *Biochemistry* **33**: 14974–14978
- Kullback S (1959) *Information Theory and Statistics*. NY: Dover Publications
- Landry SJ, Zeilstra-Ryalls J, Fayet O, Georgopoulos C, Gierasch LM (1993) Characterization of a functionally important mobile domain of GroES. *Nature* **364**: 255–258
- Lockless SW, Ranganathan R (1999) Evolutionarily conserved pathways of energetic connectivity in protein families. *Science* **286**: 295–299
- Ma J (2005) Usefulness and limitations of normal mode analysis in modeling dynamics of biomolecular complexes. *Curr Opin Struct Biol* **13**: 373–380
- Ma J, Karplus M (1998) The allosteric mechanism of the chaperonin GroEL: a dynamic analysis. *Proc Natl Acad Sci USA* **95**: 8502–8507
- Ma J, Sigler PB, Xu ZH, Karplus M (2000) A dynamic model for the allosteric mechanism of GroEL. *J Mol Biol* **302**: 303–313
- McLachlan GJ, Basford KE (1988) *Mixture Models: Inference and Applications to Clustering*. Marcel Dekker, New York
- Ming D, Wall ME (2005) Quantifying allosteric effects in proteins. *Proteins Struct Funct Bioinformatics* **59**: 697–707
- Monod J, Wyman J, Changeux JP (1965) Allosteric proteins and cellular control systems. *J Mol Biol* **12**: 88–118
- Nadler B, Lafon S, Coifman RR, Kevrekidis IG (2006) Diffusion maps, spectral clustering, and the reaction coordinates of dynamical systems. *J Appl Comp Harmonic Anal* (in press)
- Norris JR (1997) *Markov Chain*. Cambridge: Cambridge University Press
- Richardson A, Georgopoulos C (1999) Genetic analysis of the bacteriophage t4-encoded cochaperonin gp31. *Genetics* **152**: 1449–1457
- Richardson A, van der Vies SM, Keppel F, Taher A, Landry SJ, Georgopoulos C (1999) Compensatory changes in GroEL/gp31 affinity as a mechanism for allele-specific genetic interaction. *J Biol Chem* **274**: 52–58
- Richardson A, Schwager F, Landry SJ, Georgopoulos C (2001) The importance of a mobile loop in regulating chaperonin/co-chaperonin interaction: humans versus *Escherichia coli*. *J Biol Chem* **276**: 4981–4987
- Saibil HR, Ranson NR (2002) The chaperonin folding machine. *Trends Biochem Sci* **27**: 627–632
- Sewell BT, Best RB, Chen S, Roseman AM, Farr GW, Horwich AL, Saibil HR (2004) A mutant chaperonin with rearranged inter-ring electrostatic contacts and temperature-sensitive disassociation. *Nat Struct Mol Biol* **11**: 1128–1133
- Shewmaker F, Maskos K, Simmerling C, Landry S (2001) The disordered mobile loop of GroES folds into a defined beta-hairpin upon binding GroEL. *J Biol Chem* **276**: 31257–31264
- Shewmaker F, Kerner MJ, Hayer-Hartl M, Klein G, Georgopoulos C, Landry SJ (2004) A mobile loop order–disorder transition modulates the speed of chaperonin cycling. *Protein Sci* **13**: 2139–2148
- Sigler PB, Xu ZH, Rye HS, Burston WA, Fenton SG, Horwich AL (1998) Structure and function in GroEL-mediated protein folding. *Annu Rev Biochem* **67**: 581–608
- Stan G, Thirumalai D, Lorimer G, Brooks B (2003) Annealing function of GroEL: structural and bioinformatic analysis. *Biophys Chem* **100**: 453–467
- Suel GM, Lockless SW, Wall MA, Ranganathan R (2003) Evolutionarily conserved networks of residues mediate allosteric communication in proteins. *Nat Struct Biol* **10**: 59–68
- Thirumalai D, Lorimer GH (2001) Chaperonin-mediated protein folding. *Annu Rev Biophys Biomol Struct* **30**: 245–269
- Tobi D, Bahar I (2005) Structural changes involved in protein binding correlate with intrinsic motions of proteins in the unbound state. *Proc Natl Acad Sci USA* **102**: 18908–18913
- White HE, Chen S, Roseman AM, Yifrach O, Horovitz A, Saibil HR (1997) Structural basis of allosteric changes in the GroEL mutant Arg197→Ala. *Nat Struct Mol Biol* **4**: 690–694
- Xu C, Tobi D, Bahar I (2003) Allosteric changes in protein structure computed by a simple mechanical model: hemoglobin $t \rightarrow r2$ transition. *J Mol Biol* **333**: 153–168
- Xu ZH, Horwich AL, Sigler PB (1997) The crystal structure of the asymmetric GroEL–GroES(ADP)₇ chaperonin complex. *Nature* **388**: 741–750
- Yang LW, Bahar I (2005) Coupling between catalytic site and collective dynamics: a requirement for mechanochemical activity of enzymes. *Structure* **13**: 893–904
- Yifrach O, Horovitz A (1995) Nested cooperativity in the ATPase activity of the oligomeric chaperonin GroEL. *Biochemistry* **34**: 5303–5308
- Yifrach O, Horovitz A (1998) Mapping the transition state of the allosteric pathway of GroEL by protein engineering. *J Am Chem Soc* **120**: 13262–13263